Solar Absorption by Cirrus Clouds and the Maintenance of the Tropical Upper Troposphere Thermal Structure

V. RAMASWAMY

Atmospheric and Oceanic Sciences Program, Princeton University, Princeton, New Jersey

V. RAMANATHAN

Department of the Geophysical Sciences, University of Chicago, Chicago, Illinois

(Manuscript received 13 November 1987, in final form 27 February 1989)

ABSTRACT

Radiative transfer calculations employing observed values of the ice crystal size distribution demonstrate that the absorption of solar radiation by cirrus clouds can make a significant contribution to the diabatic heating of the upper troposphere. The effects due to this absorption on the upper tropospheric (100–300 mb) thermal profile are investigated in a general circulation model (GCM) with interactive clouds; guided by observations, two experiments are performed assuming vastly different vertical profiles of the ice water density. Solar heating rates within the extensive cirrus decks associated with monsoon and other convective clouds reach values of 1.5 K day^{-1}. Thus, cirrus solar heating can be an important source for east–west asymmetries in the tropical diabatic heating. Furthermore, because of the latitudinal gradients in the solar insolation, cirrus solar absorption can also influence the meridional heating gradients within the upper troposphere.

In spite of the significant east–west asymmetries in the imposed cirrus solar heating, the change in the GCM tropical temperatures is nearly zonally uniform. The magnitude of the zonal mean tropical temperature changes in the GCM (up to 5°K at $P \approx 165$ mb) indicate that lack of cirrus solar heating may be one reason for the cold bias of the GCMs. Furthermore, the shortwave heating can also account for the observed lapse rate stabilization in the upper troposphere.

In addition to the solar effect, the longwave radiative effects of cirrus can also be important but their sign and magnitude are very sensitive to the vertical distribution of clouds. Cirrus longwave heating rates can range from large negative values (cooling) when overlying optically thick clouds (for example, in "deep" extended systems with base below the upper troposphere) to large positive values (heating) for "anvil" type cirrus located in the upper troposphere and with no other clouds below. For the overcast portions of the tropics, if "anvil" type cirri are the only clouds of significance in the upper troposphere, the longwave heating would be the dominant radiative component and this effect becomes more pronounced with increasing altitude of cloud location. Hence, for the tropical zone as a whole, the sign and magnitude of the longwave effect depends on the relative composition of the "deep" and "anvil" clouds. Radiation model calculations that employ climatological values of the vertical distribution of clouds yield a longwave heating effect for the cirrus with the magnitude being comparable to the solar effect.

Thus, our results suggest a significant role for the cirrus radiative effects in maintaining the zonal mean thermal structure of the upper troposphere. This inference should be contrasted with the notion that the steep positive gradient in the tropical upper-troposphere potential temperatures is maintained by the latent heat released in penetrating cumulus towers.

1. Introduction

Clouds within the the upper troposphere, i.e., $100 \leq P \leq 300$ mb, (*referred to here as cirrus*) are known to be important components of the planetary radiative heating (Liou 1986). Radiative transfer studies (Liou 1973; Stephens 1980) have shown that the presence of high clouds would have a substantial influence on the convergence of solar and longwave radiation in the atmosphere, with the perturbations being felt throughout the column. The presence of such clouds yields large cooling (at cloudtop) and large heating (at cloudbase) rates (Ramaswamy and Detwiler 1986). The net radiative heating over a thick (2–4 km) cloud deck can range from 3–10 K d^{-1} (Fleming and Cox 1974; Houze 1982; Webster and Stephens 1980). Simulations of climate, whether in the context of local radiative heating (Manabe and Wetherald 1967) or in the context of the three-dimensional atmosphere structure (Ramanathan et al. 1983, hereafter referred to as R83) reveal a strong sensitivity to the longwave radiative properties of upper tropospheric clouds. A detailed model study of the role of cloud longwave radiative heating in the atmospheric general circulation can be found in Slingo and Slingo

Corresponding author address: Dr. V. Ramaswamy, Atmospheric and Oceanic Sciences Program, Princeton University, Princeton, N.J. 08542.

(1988). The importance of cirrus radiative effects is also evident in climate change scenarios involving increases in carbon dioxide (Manabe and Wetherald 1980; Washington and Meehl 1984).

While there is an awareness of the dependence of the upper tropospheric radiative heating on the properties of cirrus clouds, their contributions to the diabatic heating and their influence on the thermal structure are not understood. With these issues constituting the motivation for this study, the primary focus of the present paper is on the absorption of solar radiation by cirrus clouds. We begin by noting the nature of the uncertainties concerning the diabatic processes in the tropical upper troposphere, both in the context of climatological observations and in the context of climate modeling.

a. *Nature of the diabatic heating*

The diabatic forcing of the tropical upper troposphere results from convective as well as radiative processes. The convective part is primarily due to latent heat released by nimbostratus and penetrating cumulonimbus clouds associated with monsoon (e.g., Indian, Indonesian and African monsoons) and other convective systems (e.g., South American). Figure 1 shows the zonal average radiative and latent heating for the tropics estimated by Newell et al. (1974) from observed temperatures, humidity and cloud cover. The tropical heating rates shown in Fig. 1 reveal the following qualitative features: (i) The net radiative cooling and convective heating rates are of comparable magnitude such that the net diabatic heating, the term that drives the general circulation, is the result of a delicate balance between radiation and convection. (ii) The convective heating begins to decrease in the upper troposphere ($P < 300$ mb) until it becomes negligible around the tropopause ($P = 100$ mb) and radiation takes over as the dominant source for diabatic heating; and (iii) While it is reasonably certain that radiation causes a net cooling in the low to mid troposphere, i.e., $P > 300$ mb, its sign in the upper troposphere is not certain. Without the cirrus contribution, the radiation would have a net cooling effect on the upper troposphere due to emission by H_2O and CO_2. The solar absorption by cirrus would, of course, cause a heating; the longwave emission and absorption by cirrus may cause a large heating or cooling depending on the cloud characteristics and the vertical temperature distribution (Fleming and Cox 1974).

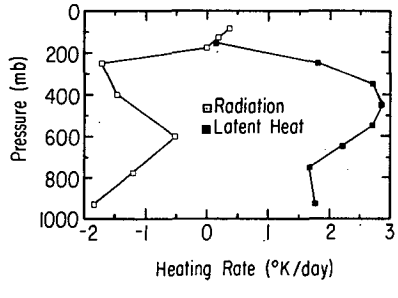

FIG. 1. Vertical distribution of the zonal mean radiative and latent heat release at the equator for the December–January–February season. Source: Newell et al. (1974). The heating rates were estimated through model calculations employing observed distributions of temperature, humidity and cloud cover.

b. *Lapse rate*

Figure 2a shows the vertical distribution of potential temperature (θ), equivalent potential temperature (θ_E) and equivalent potential temperature for a saturated atmosphere (θ_E^*) as obtained from the observed temperature and humidity distribution given in Oort and Rasmusson (1971). Figure 2b compares the lapse rate (G) for the observed equatorial profile with the moist lapse rate. Note first that the observed lapse rate (in Fig. 2b) is significantly different from the moist lapse rate throughout the bulk of the troposphere. Below 5 km, the observed lapse rate is less stable than the moist adiabatic whereas, above 9 km, the lapse rate is very stable and the departure from moist lapse rate increases dramatically with altitude. Obviously, a heat source can explain the stable lapse rates in the upper troposphere. That heat source, as described in the literature, has been assumed to be latent heat released in penetrative deep convective clouds (e.g., Riehl 1950; Newell et al. 1974; p. 46), whose base should be within the first kilometer from the surface. It is only in the surface layer that the θ_E is greater than the θ_E^* of the troposphere (see Fig. 2a), and hence the parcel has to be lifted from the surface layer for it to have sufficient buoyancy to reach the upper troposphere (e.g., see Holton 1979). While this argument is quite compelling, reliable observational estimates of the zonally averaged convective heating rates are not available to test the validity of the penetrating convective cloud hypothesis. Furthermore, the above hypothesis ignores the additional radiative effects arising due to the cirrus clouds so formed.

c. *Regional pattern of cirrus heating*

One of the most obvious manifestations of the upper tropospheric clouds in a climatological sense, is in the monthly averaged outgoing longwave flux shown in Fig. 3. Focusing again on the tropical regions, the highest emissions, i.e., values in excess of 290 W m^{-2}, are in the subsidence regions of the eastern Pacific. Under cloudless conditions, the tropical regions emit about 300 W m^{-2}. The tropical regions with emissions less than 200 W m^{-2} are unambiguously regions of extensive upper tropospheric clouds. From Fig. 3, the regions with low emissions are the monsoon regions of Indonesia, Central Africa and the deep convective region of tropical South America. The extreme low values of 160 to 180 W m^{-2} when compared with the eastern tropical Pacific value of 290 to 300 W m^{-2} suggest that

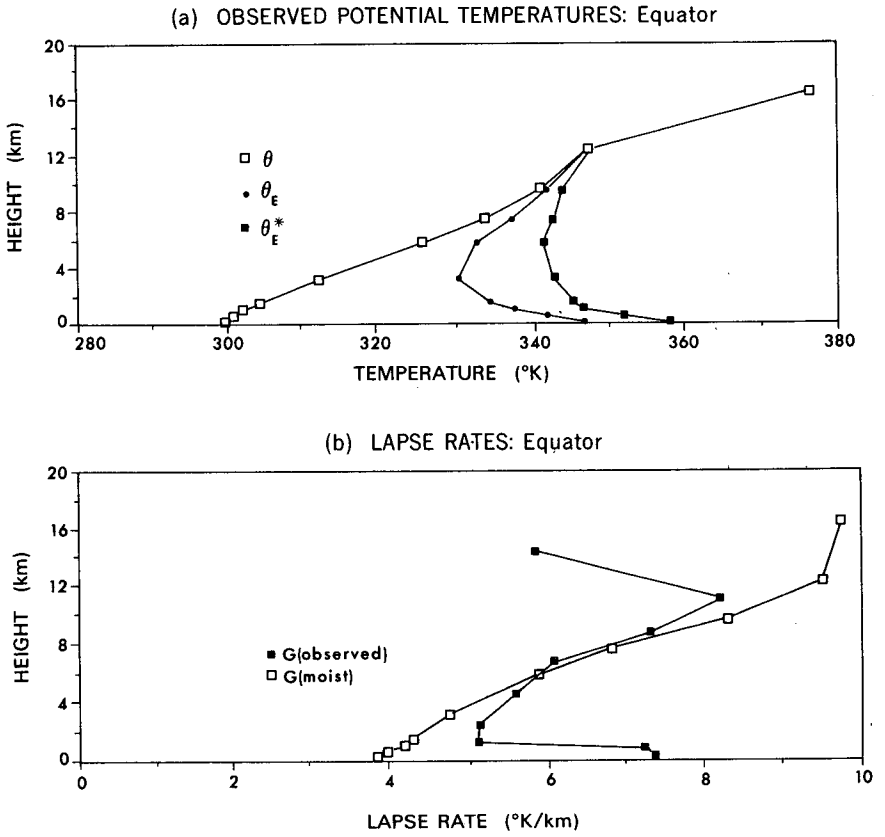

FIG. 2. (a) Vertical distribution of potential temperature (θ), equivalent potential temperature (θ_E) and equivalent potential temperature of a saturated atmosphere (θ_E^*). The values were obtained from zonal-annual mean equatorial values of observed temperatures and humidities given in Oort and Rasmusson (1971). (b) Annual zonal mean equatorial values of observed lapse rates and moist-adiabatic lapse rates. The observed lapse rates were derived from the observed temperatures given in Oort and Rasmusson (1971).

the cirrus clouds lead to a convergence of longwave radiative energy of the order of 100 W m^{-2} or more within the surface–atmosphere column. The convergence of radiative energy as revealed by the top-of-the atmosphere measurements should largely manifest itself in the troposphere (see Ramanathan 1987, for further elaboration of this point). But, the vertical distribution of the cirrus induced convergence of radiative energy is governed by the altitude of the cirrus (e.g., see Fleming and Cox 1974). Even if roughly half of the 100 W m^{-2} is assumed to represent a flux convergence in the upper 50 mb region of the upper troposphere, the resulting heating would be about 5 to 10 K day^{-1} (e.g., see Houze 1982).

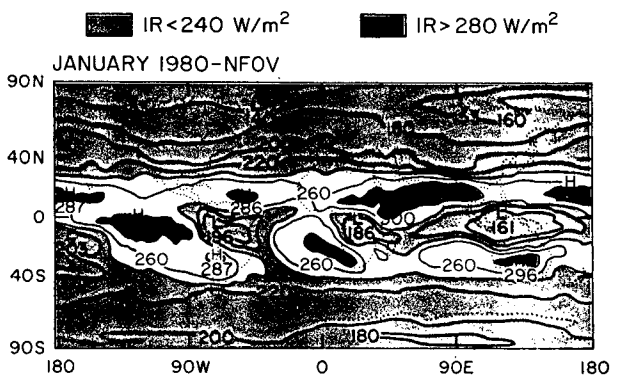

FIG. 3. Observed monthly average outoing longwave (infrared) emission for January, as obtained by the narrow-field-of-view (NFOV) scanner [Nimbus-7 Satellite (source: L. Smith, Colorado State University, private communication, 1986)].

d. *Problems with GCM simulations*

Figures 4a and 4b show the vertical distribution of the observed temperature and that of the difference between the GCM values and the observed ones at the equator for January. The observed values are taken from Oort and Rasmusson (1971). The GCM values denote an average between the computed values at 2.5°N and 2.5°S. The GCM used in this study is a version of the NCAR Community Climate Model

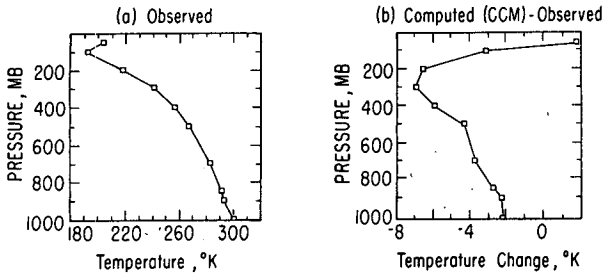

FIG. 4. (a) Vertical distribution of observed zonal mean temperature at the equator for January. Source: Oort and Rasmusson (1971). (b) Difference between the GCM computed zonal mean temperatures and observed zonal mean temperatures at the equator for January.

(CCM) described in the study of R83. The main purpose of the figure is to illustrate the cold bias in the simulation. The magnitude of the cold bias increases with altitude and reaches a peak around 200 to 300 mb. This cold bias is a persistent feature of also the earlier versions of the model (e.g., see Albrecht et al. 1986) as well as other GCMs (Mahlman and Umscheid 1984). Attempts to understand the source of the cold bias have identified the following processes:

(i) Ramanathan et al. showed that if the cirrus emissivity is arbitrarily set to 1 as in other GCMs, the clouds that form in the model (for $P < 250$ mb) absorb a significant amount of the radiation emitted by the hotter tropical surface. The net effect is to warm the upper troposphere by about 6°K and also warm the entire column. If, on the other hand, the cirrus emissivity is a function of the ice-water content in the cloud, the resultant emissivity is less than 1 and the cirrus warming of the upper troposphere is about 2°K. The inference from this study is that the radiative effect of cirrus can be significant and that the magnitude is determined by vertical moisture transport processes which govern the cirrus water content.

(ii) Following this study, Albrecht et al. (1986) included a hybrid cumulus scheme that was able to transport moisture from the lower troposphere into the upper troposphere much more efficiently than the convective adjustment. The hybrid scheme altered the latent heat release significantly such that more heat was released in the upper troposphere followed by a significant increase in the upper troposphere moisture. The net effect was a warming of the upper troposphere by about 8°K. Also, changes in convective heating were balanced by changes of opposite sign in the radiative heating. The radiative heating changes were due to an increase in moisture and an increase in clouds formed at pressure levels between 400 and 200 mb. These results should be contrasted with another CCM study by Donner (1986) which employs the Kuo-convection scheme. The Kuo-convection scheme leads to a severe cooling and drying of the tropical troposphere. However, in agreement with the Albrecht et al. (1986) study, the model response to the convection scheme was governed by interactions between convection and radiation.

e. Summary and objectives of this study

The basic inferences from the foregoing discussions are as follows: (i) the observed vertical variations of the lapse rate suggest the need for a diabatic heat source to explain the maintenance of the tropical upper troposphere thermal structure; (ii) the required heat source can be either radiative heating or latent heating or both; and (iii) since the diabatic heating in the upper troposphere results from a delicate balance between the radiative cooling and latent heating, small changes in either of the two components can result in significant changes in the tropical thermal structure. The radiative cooling results largely due to water vapor while the cirrus clouds modify the cooling. The role of cirrus longwave effects has been examined in an earlier study (R83). Accordingly, the primary objective of this study is to investigate the importance of solar absorption by ice crystals in explaining the observed thermal structure.

A one-dimensional radiative transfer model is employed to estimate the potential contributions of solar absorption, based on observed ice crystal size distributions and for the observed range in ice-water paths (section 2). Guided by these results, cirrus solar radiative properties are parameterized in the NCAR community climate model (CCM) with interactive clouds (section 3). The effects due to cirrus solar absorption on the meridional and longitudinal heating gradients and thermal structure are examined subsequently (sections 4, 5, and 6). Finally, the relative importance of the solar and longwave processes to the radiative heating of the tropical upper troposphere is examined in section 7 using the one-dimensional radiative transfer model. The principal results of this investigation are summarized in section 8.

2. Clouds in the upper troposphere and their radiative effects

a. Ice-water density profile

The condensates that form in the cold regimes of the upper troposphere ($T < 250$ K) are most likely to be ice-water mixtures or ice crystals only. The colder the temperature, the more likely it is that ice forms directly from the vapor phase, as opposed to formation from the liquid phase via freezing. The amount of condensate determines the magnitude of the radiative perturbations. In order to illustrate the vertical extent and magnitude of some typical observed condensate densities, i.e., ice water density, (IWD in g m^{-3}) in the upper troposphere, we plot in Fig. 5 the values resulting (i) from observations of Griffith et al. (1980) repre-

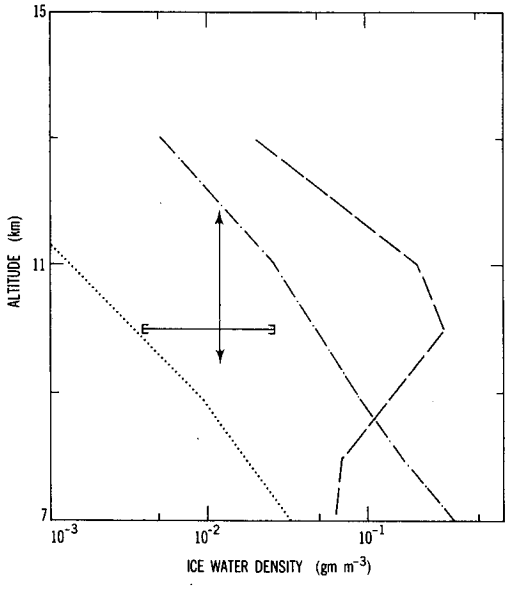

FIG. 5. Observations of ice water density in the upper troposphere: (long dashed) represents an upper limit of the observations by Griffith et al. (1980), (dot-dash) from Heymsfield (1977) for an updraft of 20 cm s^{-1}, (short dashed) from Heymsfield (1977) for an updraft of 1 cm s^{-1}; (‡) represents a lower limit of values from Griffith et al. (1980); ([—]) represents a range of values from Paltridge and Platt (1981).

senting an upper and a lower limit, respectively, (ii) from observations of Heymsfield (1977) for clouds with vertical velocities of 1 and 20 cm s^{-1}, and (iii) from observations of Paltridge and Platt (1981). The lower limits shown in Fig. 5 for the observations of Griffith et al. and those of Paltridge and Platt are a subjective estimate based on the range of values given in those references. No attempt is made here to classify the various observations according to either geographical location or the synoptic, mesoscale and small-scale conditions that initiated the clouds. The significant variability in IWD shown in Fig. 5 illustrates the difficulty in associating a characteristic IWD with cirrus clouds. For tropical cirrus in particular, the IWD, in contrast to the altitude range shown in Fig. 5, can extend up to 16 or 17 km (Kley et al. 1982). Later on, we describe the condensate densities prescribed in the GCM study.

b. Shortwave absorptivity

The solar absorption by the ice crystals in cirrus clouds is confined to the near-infrared spectrum. In order to evaluate the effects due to shortwave absorption by cirrus clouds, we compute first the absorptivity due to cirrus clouds of different optical depths (τ). For purposes of this study, we assume the ice crystal size distribution for a cirrostratus cloud (Heymsfield 1975) and further assume that each size interval can be approximated by spheres of equal surface area. Crystal lengths in this distribution range from 18 to 500 μm.

The assumption of sphericity is made for computational convenience; this is because rigorous solutions for the electromagnetic scattering by arbitrarily shaped nonspherical particles are either not available or have computational constraints. In the context of spherical scatterers, one can compare the single-scattering properties of an ice crystal distribution with that of a typical water drop size distribution. Typically, in the near infrared wavelengths, the ice distribution has a smaller single scattering albedo than a water drop distribution. The solar spectrum weighted single-scattering coalbedo, i.e., the single scattering albedo subtracted from 1, which is an approximate indicator of the solar absorption by the crystal at each scattering event, is 0.05 for the cirrostratus distribution; this is to be contrasted with values 0.01–0.02 for typical water clouds (Charlock and Ramanathan 1985; Chylek et al. 1984). The primary cause of the increased absorption in the case of ice crystals is their larger size. Increased absorption at each scattering event translates into an increase in the solar flux absorbed by the cloud. It is pointed out that yet another distribution (cirrus uncinus) is reported by Heymsfield (1975), which contains larger particles (up to 2000 μm in length) and yields a factor of two greater value of coalbedo than the cirrostratus distribution employed in the present study. It is also worth mentioning at this stage that some speculation exists about the presence of sizes smaller than those observed; details about this issue have yet to be ascertained.

The shortwave absorption by the assumed ice crystal distribution is calculated using the refractive indices of Warren (1984), Mie calculations and the delta-Eddington approximation (Wiscombe 1977). In Fig. 6a, we plot the shortwave absorptivity due to the cirrostratus distribution, as a function of ice-water path (IWP) in the range 0–70 g m^{-2}, which corresponds to an extinction optical depth range of 0 to 5 at a wavelength of 0.5 μm. Five different zenith angles are considered. The absorptivity increases with increasing optical depth (τ) and, for $\tau < 3.0$, it increases with increasing zenith angle. At $\tau = 1.5$, the absorptivity is 5% for cosine of zenith angle of 0. 6. The values of the absorptivity agree well with those deduced from observations of clouds with comparable IWP (Paltridge and Platt 1981). Cirrus absorptivities of $\sim$0.05 are also obtained by Liou and Wittman (1979) based on the scattering properties of cylinders.

c. Column shortwave heating

The computations employ a one-dimensional radiative transfer model (Ramaswamy and Kiehl 1985) with a tropical atmospheric profile of gases (O_3, CO_2, H_2O) and relevant meteorological parameters (temperature, density, pressure), based on McClatchey et al. (1972). Three levels of clouds are considered (Manabe and Wetherald 1967)—low (fraction = 0.34,

cloudtop 3 km), middle (fraction = 0.08, cloudtop 6 km) and high (fraction = 0.23, cloudtop 13 km). The optical depth at 0.5 μm for the low cloud is 10, that for the middle is 13.6 while that for the high cloud is considered an independent variable here. Clouds are assumed to be randomly overlapped. Fifty-six spectral intervals are considered for the shortwave radiative transfer, of which 9 are in the near-IR spectral regime. Water vapor absorption is treated using the exponential sum fits of Liou and Sasamori (1975); further details can be found in Ramaswamy and Kiehl (1985). Single-scattering characteristics of the low and middle clouds in each spectral interval are assumed to be represented by an altostratus drop-size distribution (Chylek et al. 1984). The magnitude of the shortwave heating for the layer containing a cirrus cloud between 12 and 13 km is shown in Fig. 6b for the same extinction optical depths considered in Fig. 6a. The heating rates refer to a layer 1 km thick. The cosine of the solar zenith angle is assumed to be 0.6 while the fraction of the day is 0.5. Also shown in Fig. 6b are the heating resulting due to a nonabsorbing cloud (coalbedo is 0), and that due to a cloud with distribution similar to that of an altostratus cloud (i.e., a water cloud). The significance of varying the optical depth here implies that, while the extinction optical depth is the same in all three cases, the scattering and absorption optical depths for the different cases vary due to the three different coalbedo values (in each of the near-infrared spectral intervals considered in the model). This arrangement enables a quantitative assessment of the effect of single-scattering albedo. According to this arrangment, an optical depth of zero essentially implies the absence of a cloud in the upper troposphere, and the heating in this case is solely due to water vapor absorption.

First, considering the nonabsorbing cloud, the increase in the optical depth leads to an almost negligible

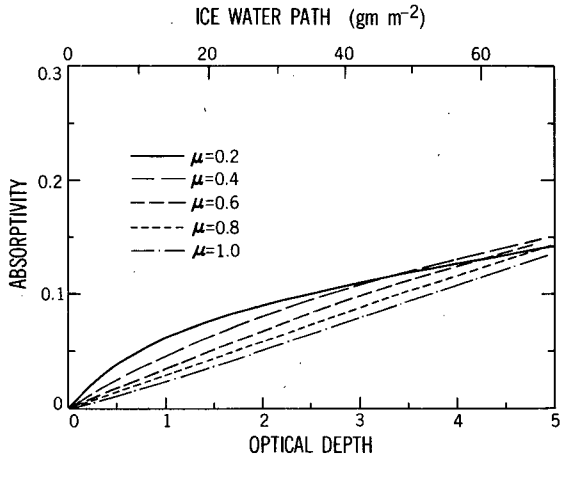

FIG. 6a. Shortwave absorptivity of a cirrus cloud (cirrostratus size distribution) as a function of ice water path (or optical depth) for five different cosines of solar zenith angles (μ).

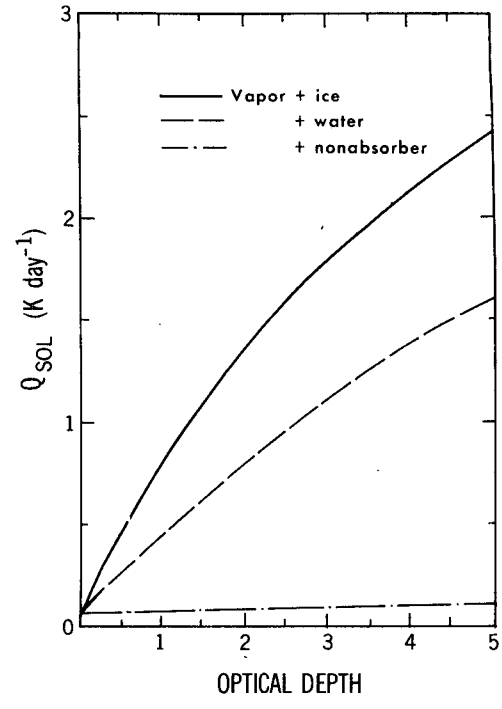

FIG. 6b. Shortwave heating rate in a 1 km thick cirrus cloud with cloudtop at 13 km in a tropical atmosphere (McClatchey et al. 1972), as a function of cloud extinction optical depth. (dot dashed) represents the case when particulates are assumed to be nonabsorbing, (long dashed) represents the case when particles have single-scattering characteristics of a water cloud while (solid) represents the case when the particles have single-scattering characteristics of ice crystals.

increase in shortwave heating (for all τ, $Q_{sol} < 0.12$ K d^{-1}). The increase is due to increased photon path length resulting in increased water vapor absorption. Owing to low water vapor mixing ratio at the considered altitude, these increases are minimal. Next, considering the water drop distribution, the heating increases with τ to a value of 0.64 K d^{-1} for τ = 1.5 and 1.6 K d^{-1} for τ = 5.0.

The cirrostratus distribution yields a heating of 1.1 K d^{-1} at τ = 1.5 and 2.4 K d^{-1} at τ = 5.0. Enhancement with respect to the water drop distribution can be up to ~70%. The absence of shortwave absorption due to other constituents in the upper troposphere (because of low water-vapor amounts, low carbon dioxide and ozone absorptivities) emphasizes the importance of the perturbations due to cirrus clouds. Note that, if a layer of the same geometrical thickness is considered at a higher altitude, the heating would be further enhanced.

Next, we inquire about the significance of keeping the ice-water content fixed, and varying the optical depth. In this case, a fixed condensate amount is assumed to be distributed among either a predominantly large particle distribution (such as ice crystals) or a relatively small particle distribution, such as a typical water cloud. The principal differences between the two cases are not only a higher single scattering albedo for

the smaller particles (as noted earlier) but also a higher specific extinction. For instance, the specific extinction of an altostratus cloud drop size distribution (Chylek et al. 1984) is more than three times that for the cirrostratus distribution (0.24 vs 0.07 $m^2 g^{-1}$) in the visible spectrum. This implies that for a given IWP, the extinction optical depth for the smaller distribution will be more than three times that for the cirrostratus. The heating rate for the two types of particle distributions under the constant ice water path assumption is shown in Fig. 7. For IWP < 15 g m^{-2}, the lower coalbedo of the smaller particle distribution is more than offset by the increase in optical depth so that the resulting absorption and, thus, the heating are similar for both distributions. However, for larger IWPs, the smaller particle distribution approaches saturation values which are less than that of the larger particle distribution. This particular example emphasizes the need to resolve the issue concerning the presence of smaller particles in the ice crystal distribution and to assess accurately the single-scattering parameters of cirrus clouds.

The details of the radiative characteristics for all types of cirrus systems cannot be universally formulated at the present time owing to inadequate observations, lack of knowledge on their microphysical aspects and theoretical limitations of electromagnetic scattering by the nonspherical ice crystals. What can be gleaned at present from Figs. 5, 6 and 7 is the potential for substantial solar radiative heating in the upper troposphere by clouds containing ice crystals.

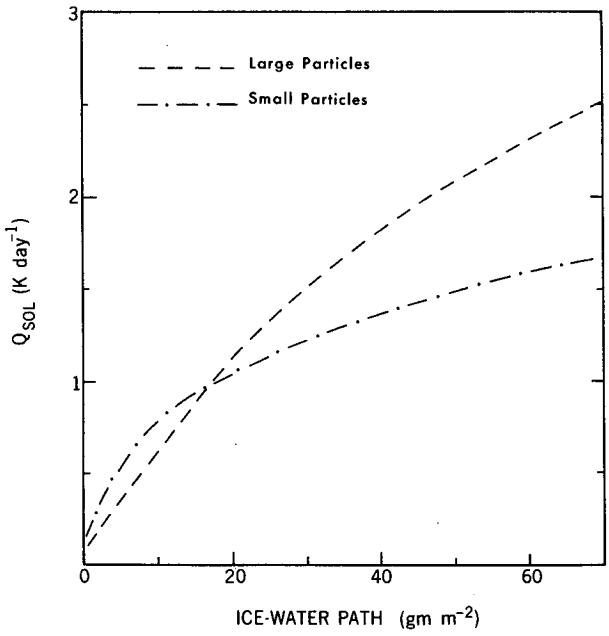

FIG. 7. As in Fig. 6b except for constant ice-water path in the case of a cirrostratus distribution comprised of large particles and an altostratus water drop distribution comprised of relatively smaller particles. See text for further details.

3. The GCM experiments

The model used in this study is a modified version of the NCAR community climate model (CCM0) described by Pitcher et al. (1983). The modifications are described in Williamson et al. (1987) and a brief description of the modifications is given below. The finite difference method used in formulating the equations in the vertical has been changed from that used in CCM0 in order to be formally energy conserving. The vertical resolution has been changed from 9 levels in CCM0 to 12 levels in the present version. The additional three levels have been added between 500 and 50 mb to better resolve the upper troposphere and lower stratosphere regions. The radiation treatment was substantially altered, particularly in the treatment of water vapor, where the scheme described by Kratz and Cess (1985) was used for the solar absorption and that by Ramanathan and Downey (1986) for longwave emission. The ozone longwave absorption follows Ramanathan and Dickinson (1979) and the CO_2 longwave parameterization was modified slightly by Kiehl and Briegleb (private communication; also described in Williamson et al. 1987). Furthermore, clouds are allowed to form in all layers of the model up to 100 mb and the longwave emissivity of clouds follows the liquid water scaling of R83. The scheme for forming clouds in the model is, otherwise, as described in R83.

Three important modifications to the radiation scheme in the shortwave spectrum are effected for purposes of the present study. The cloud radiative treatment is modified to include explicitly the absorption by ice crystals in the uppermost cloud layer. Second, the coefficient used in computing the reflectivity of the highest cloud layer [see Eq. (16) in R83] is adjusted to correspond to that of an ice crystal distribution. Third, shortwave absorptivity and reflectivity of cirrus are parameterized as a function of extinction optical depth (τ) at a wavelength of 0.5 μm and cosine of the solar zenith angle, and are explicitly evaluated in the code. In the parameterization, the coefficient obtained for reflectivity is 0.125, in contrast to 0.15 used in R83. The expression for the absorptivity is presented in Appendix A with

$$\tau = 0.074 \times \text{IWP}.$$

The value of 0.074 $m^2 g^{-1}$ is the specific extinction obtained for the assumed ice crystal distribution while IWP is the vertical ice-water path in g m^{-2}.

Cirrus clouds, for the purpose of incorporating the cloud shortwave absorption in the GCM, are introduced according to the following criterion: whenever the temperature in any layer (except the top) falls below 250 K and a cloud is formed in that layer by the model, it is deemed to be a cirrus cloud with an optical depth as defined above.

We perform two sets of sensitivity studies with different prescribed ice-water density profiles. In the first

set (designated as fixed content or FC), any layer in which a cirrus cloud occurs is assigned an IWP of 20 g m^{-2} (see values listed for various layers in Table 1). In the second set (designated as variable content or VC), layers have assigned to them values of IWP which decrease with increasing altitude as shown in Table 1. Note that variability, as denoted here, is with respect to layers.

With respect to the observed profile displayed in Fig. 5, the FC and VC cases, as defined above, should yield a high and a low value, respectively, (not necessarily limiting values) for the shortwave radiative effects above 15 km; between 15 and 11 km, FC values are between the range observed; below 11 km, both FC and VC values become less and lie near the lower limit of observed values.

Note that in the FC case, the optical depth in all layers containing cirrus clouds is fixed (see Table 1) at 1.5 while that in the VC case is variable and ≤ 1.5. Thus, FC values are always equal to or greater than VC values. Since absorptivity is a monotonically increasing function of optical depth (Fig. 6a), differences in τ translate into differences of the same sign in absorptivity. The longwave cloud properties, for purposes of reference to the earlier results, are allowed to vary according to the methodology described in section 6 of R83.

4. Cirrus solar radiative forcing: GCM results

The CCM sensitivity results described here were started from day 200 of the model control run. The control run was started from day 1 with arbitrary initial conditions and integrated for 350 days with perpetual January solar insolation and sea-surface temperatures. The sensitivity runs were started from day 200 and integrated for 150 days. In this section, we describe the time average solar heating rate differences, which can be considered as the radiative forcing for interpreting the sensitivity runs. Unless otherwise mentioned, all of the results pertain to time averaged values obtained from the last 90 days of the 150 day runs of the control and the sensitivity experiments.

First, we analyze the FC case. Zonal averages of the model cloud cover are shown in Fig. 8a which indicate a maximum value of 0.15 in the tropics at ~200 mb, decreasing to 0.05 at approximately 100 mb. The decrease in the height of the cirrus clouds in going from tropics to the high latitudes accompanies the decrease in tropopause height. The cloud distribution for the control run is similar to that shown in Fig. 8a except that the control has more upper level clouds. The reasons for the decreased cirrus clouds are mentioned later.

The change in the zonally-averaged shortwave heating rate (K d^{-1}) due to near-IR cirrus absorptivity is shown in Fig. 8b. In order to facilitate visual perception of the results, we display only those regions with heating rate differences larger than 0.1 K d^{-1}. As is to be expected, a one-to-one correspondence exists between the regions of maximum cloud cover and the regions of maximum heating perturbation. The changes in the heating rate are largest in the uppermost cloud layers. The maximum value induced by the shortwave absorption is ≈ 0.5 K d^{-1} at $P \approx 165$ mb in the equatorial upper troposphere. A secondary maximum of ≈ 0.3 K d^{-1} occurs at $P \approx 350$ mb in the midlatitudes of the SH. Since the plots are for January insolation conditions,the cloudy regions in NH midlatitudes, where the solar insolation is smaller, show comparatively negligible perturbations in the heating rates.

Since the largest perturbations occur at 165 mb, we show in Fig. 9 the latitude–longitude cross section of the radiative perturbation at this level. It is seen that the contribution to the zonally-averaged radiative heating by high clouds in the shortwave comes principally from localized regions of intense heating, as opposed to a zonally distributed source. From Fig. 9, these appear to be located in the South American and the African continents, and in the Asian monsoonal regions where the maximum solar heating is 1.5 K d^{-1}. The regions of maximum heating in the tropics coincide with regions of minimum outgoing longwave emission in the observed values shown earlier in Fig. 3. The coincident pattern in the computed solar heating maximum and the observed emission minimum lends

TABLE 1. Ice water density (IWD, g m^{-3}), ice-water path (IWP, g m^{-2}) and optical depth (τ) of cirrus clouds in the different GCM layers. Two different vertical profiles (fixed content, FC and variable content, VC) are considered. τ is the extinction optical depth at a wavelength of 0.5 μm.

			FC			VC		
σ-level*	Layer** top (km)	Layer base (km)	IWD (g m^{-3})	IWP (g m^{-2})	τ	IWD (g m^{-3})	IWP (g m^{-2})	τ
60	21.8	17.5	0	0	0	0	0	0
110	17.5	15.0	8.0×10^{-3}	20	1.5	4.0×10^{-4}	1	0.07
165	15.0	12.3	7.4×10^{-3}	20	1.5	1.9×10^{-3}	5	0.37
245	12.3	9.5	7.1×10^{-3}	20	1.5	3.6×10^{-3}	10	0.75
355	9.5	7.0	8.0×10^{-3}	20	1.5	8.0×10^{-3}	20	1.50

* Mid-cloud location.
** Approximate heights using U.S. standard atmospheric scales.

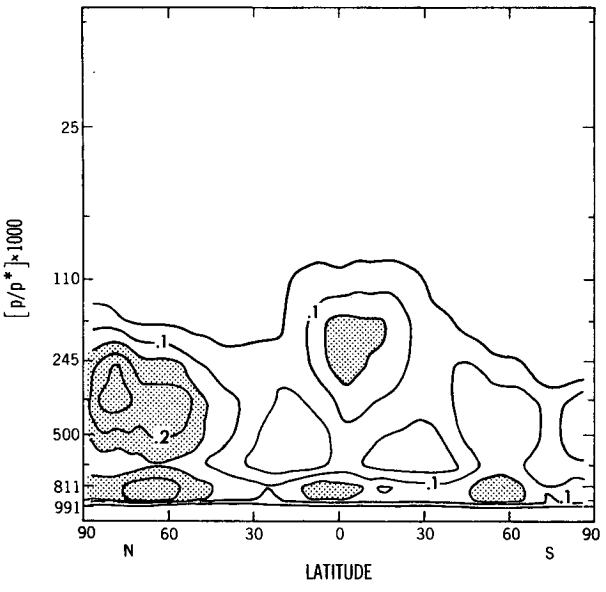

FIG. 8a. Zonally averaged cloud cover, as obtained from the NCAR CCM for January conditions. Contour interval is 0.05 and values greater than 0.15 are shaded.

some credence to the model's simulation of the geographical pattern of cirrus clouds, since regions with minimum emission are also regions of maximum cirrus cloud cover.

We next investigate the typical vertical profile of the shortwave radiative perturbations at an equatorial latitude. For this purpose, we choose 2.5°S and show in Fig. 10a the zonally averaged cloud cover and in Fig. 10b the zonally-averaged heating with and without cirrus solar absorption. The cloud cover at this latitude consists of a partial cloud cover in all layers which can be classified, broadly speaking, into a high cloud (fraction 0.18 at 250 mb), middle (maximum fraction of 0.075 at 500 mb) and low (maximum fraction of 0.17 at 800 mb). From Fig. 10b, the shortwave heating at 200 mb without considering the near-IR crystal absorption is $\approx$0.28 K d^{-1}. The influence of the near-IR absorption increases the heating at this level to 0.7 K d^{-1}—i.e., the upper level heating is perturbed by more than a factor of 2. The changes due to the ice absorption are confined to above 500 mb (change at 500 mb is <10%). Below this level, negligible increase and even a decrease is seen in the shortwave heating due to two reasons: (i) temperatures at lower altitudes increase to above 250°K for which (see section 3) no near-IR absorption is prescribed (although, in a strict sense, the near-IR absorption for water drops at these warmer temperatures ought to be included); and (ii) in the presence of ice crystals, less radiation is available for absorption at the lower levels. The radiative energy available for absorption below 650 mb is reduced so that there is less heating between this level and all the way down to the surface.

The VC case, because of a deliberate underestimate of IWD, will yield a lesser perturbation than the FC case. The zonally-averaged perturbation in the shortwave radiative heating is shown in Fig. 11 for the VC case. Relative to the cloud cover (Fig. 8a) and the heating rate perturbation for the FC case (Fig. 8b), the maximum perturbation in the equatorial upper troposphere is less (~0.15 K d^{-1} at 300 mb). At 165 mb, the perturbations are less by a factor of 5 compared to the FC case. Another significant difference with respect to the FC case is the lowering of the maximum heating to 300 mb (it was 165 mb in the FC case). As seen earlier, only the upper tropospheric layers of tropical cloud systems absorb the radiation in the near-infrared because of the prescription of only ice crystal absorption in the present work.

For the cloud systems in the mid- to high-latitudes of the Southern Hemisphere, the heating profile is approximately similar in both VC and FC cases. This is because the IWD and the optical depth prescribed at 245 mb differ by only a factor of two between the FC and VC cases, while for $P > 245$ mb, they are identical in both cases. Since clouds in the middle and high latitudes occur mainly when $P > 245$ mb, the heating rates for the FC and VC cases at these latitudes are similar. For $P > 400$ mb, the heating rate profiles are again comparable for the two cases. In the VC case too, a reduction in heating perturbation occurs in the lowest few layers (e.g., $P > 750$ mb at 20–40°S) owing to the radiative properties of the ice crystals in the layers above. Finally, it is pointed out that had we chosen a distribution of ice crystals that are smaller in size (sim-

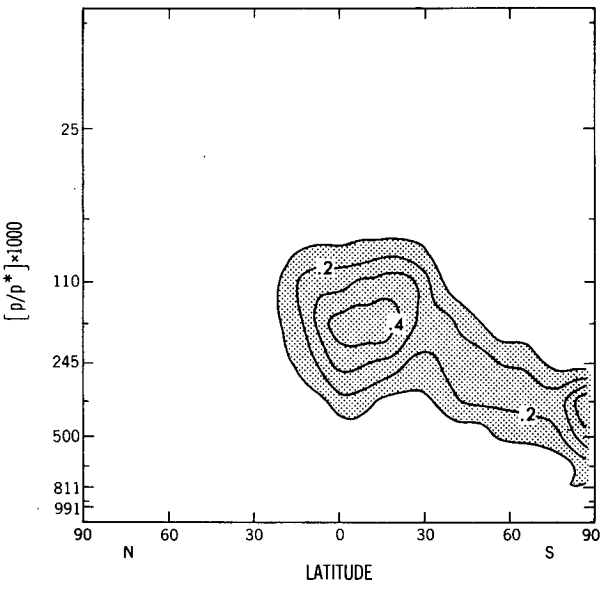

FIG. 8b. Zonally averaged (January) change in the shortwave heating rate due to cirrus absorption (fixed content case). Contour interval is 0.1 K day^{-1}. Maximum changes occur near the equatorial and summer hemisphere tropopause.

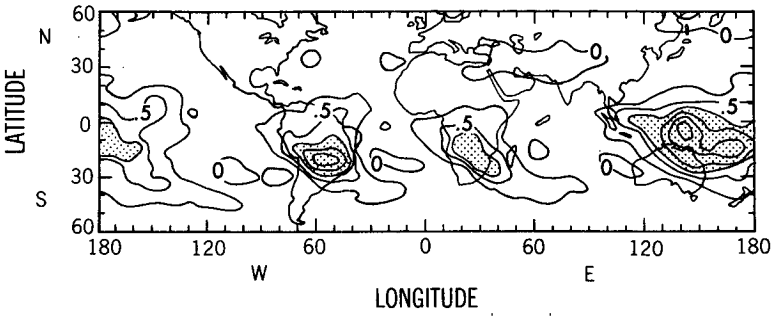

FIG. 9. Change in the heating rate at 165 mb (January) due to cirrus absorption (fixed content case). Contour interval is 0.25 K day^{-1}. Regions greater than 0.75 K day^{-1} are shaded. Maximum change occurs in the winter monsoonal regions ($\approx$1.5 K day^{-1}).

ilar to, say, a water drop-size distribution), the heating rate perturbations could be smaller, as seen in Figs. 6b and 7.

5. Radiative response of the atmosphere to cirrus solar heating

In order to facilitate interpretation of the GCM results concerning the thermal response of the tropical upper troposphere to cirrus-induced solar heating (described later in section 6), we estimate the purely radiative response. This is done by invoking the so-called fixed dynamical heating concept employed by Fels and Kaplan (1975) and Ramanathan and Dickinson (1979). This is a useful concept to evaluate the temperature response of the atmosphere in the limit of constant dynamical heating. Starting from an atmosphere in a prescribed radiative–dynamical equilibrium, we determine the response of the zonally averaged tropical atmosphere to an imposed zonally-averaged upper tropospheric radiative heating perturbation when only the temperature is allowed to change, i.e., the water vapor profile, the surface temperature and all other atmospheric properties, including the dynamical heating, are held fixed. The resulting change in the upper tropospheric temperature will then be the adjustment, through longwave radiation, to the imposed perturbation, i.e., the atmospheric temperature increases until the increased longwave cooling balances the imposed heating. Cloud optical properties, through their effect on the longwave radiative transfer, can be

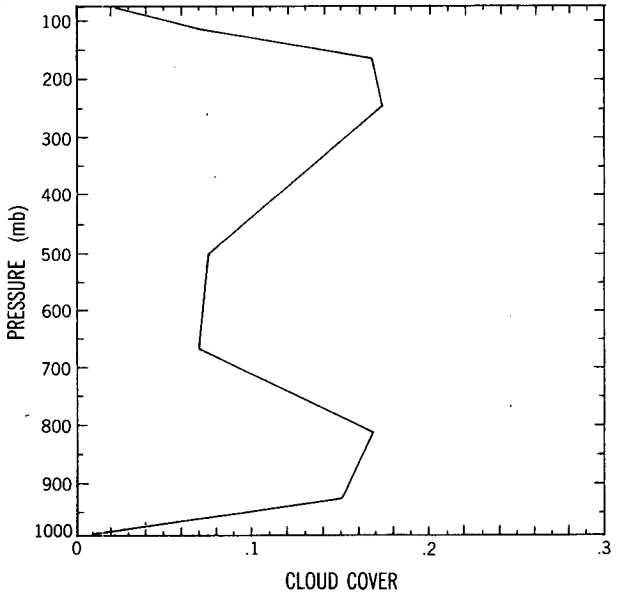

FIG. 10a. Vertical profile of cloud cover (January) at 2.5°S, as obtained from the NCAR CCM.

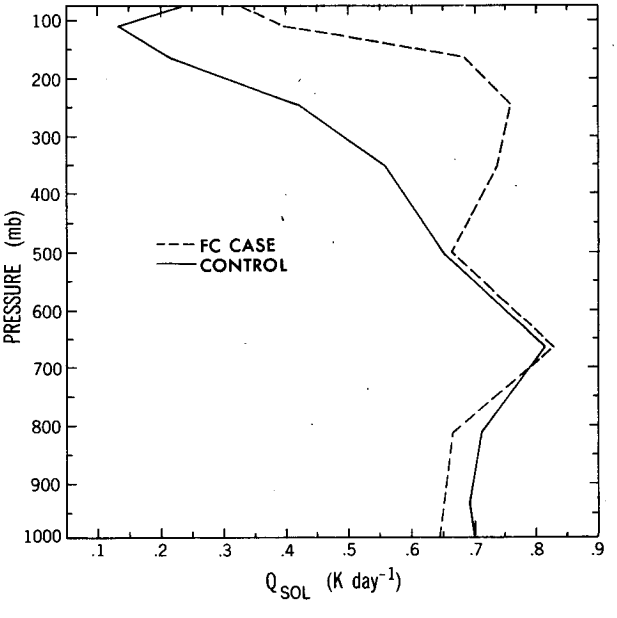

FIG. 10b. Solar heating rate at 2.5°S (January) without (solid) and with (short dashed) cirrus shortwave absorption (fixed content case). A pronounced increase occurs above 500 mb while a decrease occurs below 700 mb.

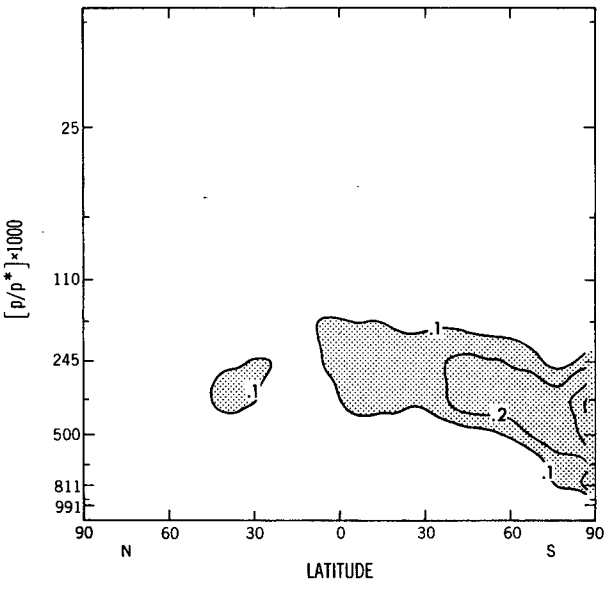

FIG. 11. Zonally averaged (January) change in the shortwave heating rate due to cirrus absorption (variable content case). The cloud cover is shown in Fig. 8a.

expected to affect the adjustment process. Note that, in the context of the fixed dynamical heating, the source of the heating perturbation can be regarded very generally and can be considered to arise from a host of causes, one of which is the cirrus shortwave absorption.

The time-marching, one-dimensional model and the methodology used to determine the radiative response are outlined in appendix B. As a guide to the sensitivity of the response, we choose two cloudtop pressures (165 and 217 mb) and a solar radiative forcing of 0.5 K d^{-1}. In each case, the cloud is in an ~1.5 km thick layer. The altitudes and the forcing are representative of the zonally-averaged cirrus-induced solar perturbations in the tropics that have been described earlier in section 4. It is worthwhile noting that the longwave heating perturbation within the upper troposphere due to cirrus clouds having an emissivity of unity, with prescribed cloud cover was found to be (see R83) approximately 0.5 K d^{-1} (between 30°S and 30°N).

The change in the equilibrium radiative response (ΔT_{rad}) is shown as a function of the "grey" cloud emissivity (ϵ) in Fig. 12 at the two altitudes. The temperature increase due to the heating when the cloudtop is at 165 mb varies from 6.3°K (for $\epsilon = 0$) to 3.2°K (for $\epsilon = 1$). The response is larger for smaller values of the emissivity. If the heating is at a lower altitude (cloudtop at 217 mb), the reponse is weaker (3.8°K at $\epsilon = 0$ to 2.3°K at $\epsilon = 1$).

The dependence of the temperature response on cloud emissivity can be understood as follows. The emission by the layer containing the "grey" cirrus increases linearly with emissivity. Hence, the required increase in the longwave emission (to balance the imposed heating) can be met with a smaller temperature change for a cloud with larger emissivity. One additional point must be noted regarding the radiative adjustment. Since the response depends on the longwave absorption properties at the altitude considered, other radiative constituents, whose concentrations are a function of space and time (e.g., ozone, aerosols, water vapor), may become relevant as well in the radiative adjustment of the tropical upper troposphere to a heating perturbation.

6. GCM temperature response

The computed perturbation to the zonally-averaged temperature field for the FC case is shown in Fig. 13. It is seen that the tropical upper tropospheric temperature shows an increase in approximately the same latitude regime where the radiative heating perturbations occur (see Fig. 8b). However, the altitude of maximum temperature perturbation lies above that of the maximum heating perturbation. Another feature is the pronounced cooling in the polar lower stratosphere which is difficult to interpret as considerable variability exists in that region during winter owing to planetary wave activity (Mahlman and Umscheid 1984; Boville 1987). However, the increase in the upper tropospheric equator to pole temperature gradient, in response to the

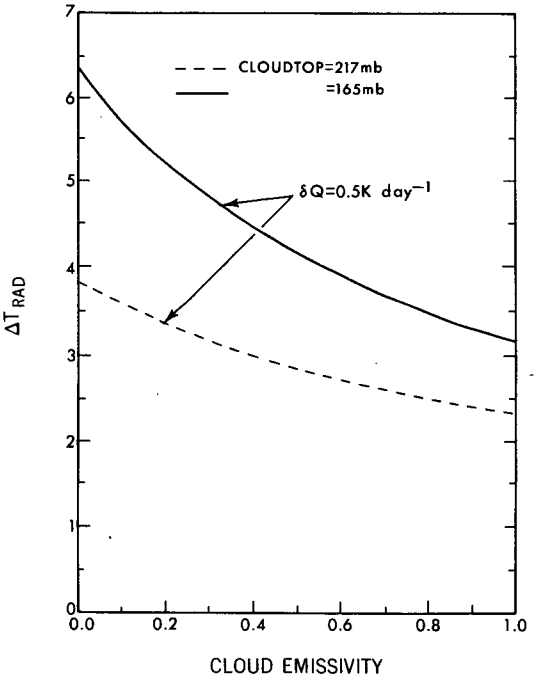

FIG. 12. Change in temperature as a function of high cloud emissivity due to an imposed cirrus solar heating of 0.5 K day^{-1} in a one-dimensional model with fixed dynamical heating. Cloud top altitudes are chosen to be 165 or 217 mb. The calculations are performed for a tropical profile (McClatchey et al. 1972). See text for details.

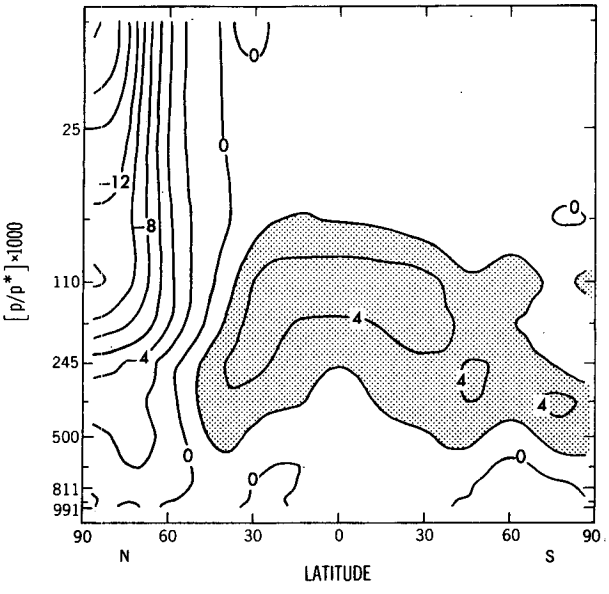

FIG. 13. Zonally averaged (January) change in temperature due to cirrus absorption (fixed content case). Contour interval is 2°K. See Fig. 8b for the corresponding heating rate perturbation.

enhanced solar heating gradient, is consistent with linear dynamical theory. The relevant arguments are given in Fels (1985) and in Ramanathan (1987), and follow from the particular form of the transformed Eulerian mean equations given in Plumb et al. [1986; Eqs. (10.9) and (10.11)]. The physical arguments proceed as follows. The upper tropospheric radiative response to an enhancement in the radiative heating gradient (see Fig. 8b) is an enhanced temperature gradient. Through geostrophic balance, this would lead to an increase in the strength of the westerly winds. This, in turn, can alter the planetary wave propagation through its dependence on the strength and shear of the zonal mean winds.

Looking at the response in the tropics, the near-IR absorption by cirrus clouds acts to heat the upper troposphere. Since considerable uncertainty exists in the knowledge on the optical properties of ice droplets, this uncertainty could very well be a principal cause of the inability of GCMs to simulate observed tropical tropopause temperatures (Albrecht et al. 1986; Mahlman and Umscheid 1984). The maximum perturbation to the temperature occurs at the 165 mb level. and the regional distribution of the change is shown in Fig. 14. The temperature increases (maximum of about 5°K) are considerably uniform in a zonal sense, in contrast to the concentrated geographical location of the radiative heating perturbation (see Fig. 9). The zonal nature of the temperature response is to be compared with the observed pattern of tropical upper troposphere temperatures which exhibits very little regional asymmetry (Newell et al. 1974).

To obtain an idea of the GCM response time for the tropical upper troposphere, we show the temperature difference in the vertical column at 2.5°S (Fig. 15); this is to be compared with the heating rate shown in Fig. 10b. At 165 mb, a ΔQ of $\approx$0.42 K d^{-1} yields a ΔT of 4.2°K, yielding a time constant of approximately 10 days; this is well within the range of the radiative response obtaned in section 5 (3.2 to 6.3°K warming due to a 0.5 K d^{-1} imposed heating). This suggests that the response to the perturbations in the GCM's upper troposphere may be largely radiative. It is also interesting to note from Fig.15 that, the temperature change peaks between 100 to 150 mb, although from Fig.10b, the heating rate perturbation in this layer is much smaller than that between 150 to 200 mb. The greater temperature sensitivity of the upper layer is partly due to the increase in the radiative temperature

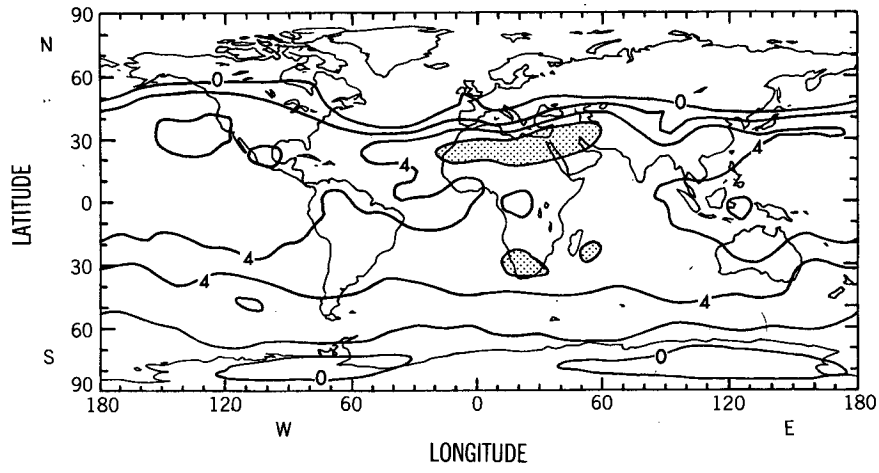

FIG. 14. Change in temperature at 165 mb (January) due to cirrus shortwave absorption (fixed content case). Contour interval is 2°K; only positive contours are drawn. See Fig. 9 for the corresponding heating rate perturbation.

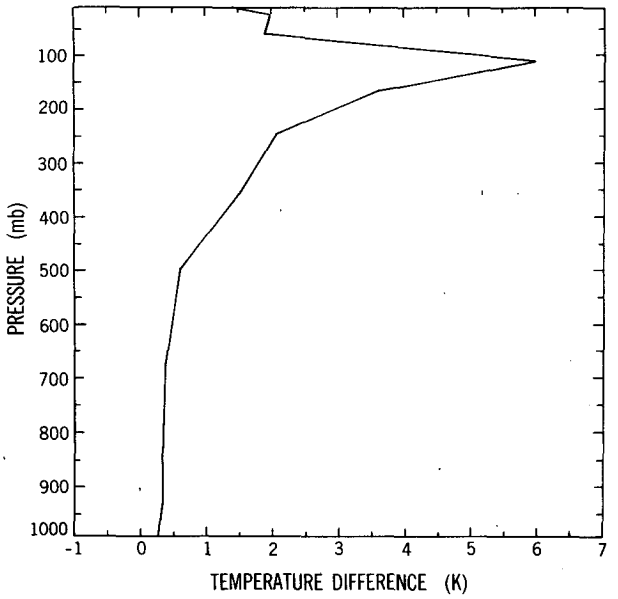

FIG. 15. Change in temperature at 2.5°S (January) due to cirrus shortwave absorption (fixed content case). See Fig. 10b for the corresponding heating rate perturbation.

response with altitude within the upper troposphere (see section 5). However, we caution that, as shown in section 5 (Fig. 12), the thermal response is significantly sensitive to the emissivity of cirrus clouds.

The perturbation to the temperatures for the VC case (not shown here) is substantially smaller than that in the FC case. For example, the maximum temperature change in the tropical upper troposphere is about 1°K.

We have thus far not mentioned an important feature concerning the present GCM simulations. As one may expect, the response to the large initial shortwave heating in a realistic atmosphere would have to produce a decrease in cloudiness (because of decrease in relative humidity due to the increase in the temperatures), in the absence of enhanced convective transport. This does indeed occur in our simulations with the cloud cover at 165 mb (tropics) in the FC case decreasing by ~0.02 (10%). There is, in general, a decrease of cloud cover in the entire tropical upper troposphere for the FC case. Both for lower and middle troposphere in the FC case and for the entire troposphere in the VC case, the feedbacks due to and upon the cloudiness are not readily interpreted because of the arbitrary way in which IWD has been prescribed in this study. It is admittedly a complicated task to interpret cloud feedback mechanisms in the upper troposphere and is beyond the scope of the present sensitivity study. However, an important point that must be gathered from the present GCM simulations is the degree to which the cirrus shortwave absorption affects the thermal profile of the upper troposphere.

Finally, the magnitudes of temperature change obtained are approximately similar to the deficit in the GCM tropical temperatures when compared with observations (see Fig. 4b). Thus, the characteristics of ice clouds can play an important role in determining the temperatures around the tropical tropopause. Further, if absorption by ice crystals is one of the causes of the GCM's "cold" bias in the tropics, then the vertical profile of the IWD and its magnitude become a significant factor for explaining the observed lapse rate stabilization in the tropical upper troposphere (see Fig. 2b).

7. Relative importance of cirrus solar and longwave effects

The longwave radiative effect of cirrus on the upper troposphere (10 to 17 km) temperature can be as large as, or even larger than, the solar effects discussed in this study (e.g., see R83; Slingo and Slingo 1988). Both solar and longwave heating rates depend on a number of atmospheric and cloud parameters (listed in Table 2), some of which are poorly known. Hence, climatological distribution of the heating rates are highly uncertain. In the case of the cirrus longwave effect, the problem is further complicated because, not only the magnitude but also the sign of the effect (whether heating or cooling) depends on poorly known parameters such as cloud top and base altitudes. For example, it can be deduced from the radiation model calculations of Fleming and Cox (1974) and others (e.g., Stephens 1980; Ackerman et al. 1988) that the longwave effect of a cirrus cloud can change from a net heating to a net cooling just by lowering either the cloud top or the cloud base altitude.

The aforementioned studies show that the cirrus longwave effect is essentially due to the difference between the upwelling flux from below the upper troposphere and that emerging at the cirrus boundaries.

TABLE 2. Parameters which govern directly the magnitudes of solar and longwave heating rates in the tropical upper troposphere ($100 \leq P \leq 300$ mb).

Parameter	Solar heating	Longwave heating
Vertical profile of ice water path	yes	yes
Ice crystal shape and size distribution	yes	yes
Solar zenith angle	yes	—
Surface albedo	yes	—
Cloudtop altitude	yes	yes
Cloud geometrical depth	yes	yes
Clouds between 300 mb and surface	yes	yes
Cloud geometry	yes	yes
Cloud fraction*	yes	yes

* For zonal considerations.

The upwelling flux is very sensitive to the vertical distribution of the clouds. It is a minimum for cirrus clouds that are part of an optically thick system extending from the lower troposphere ("deep" clouds), while being a maximum for "anvil-type" shallow cirrus clouds located in the upper troposphere of an otherwise clear atmosphere. While the deep clouds will always lead to a longwave cooling of the upper troposphere (e.g., see Cox and Griffith 1979), the anvil cirrus can lead to a longwave heating depending on its top and base altitudes (e.g., Fleming and Cox 1974). This sensitivity to cloud altitude, when combined with the uncertain knowledge of the climatological cloud altitudes, precludes a rigorous assessment of the relative importance of the longwave and solar effects of cirrus.

The above uncertainties notwithstanding, we attempt here to compare the relative magnitudes of the solar and the longwave effects. The sensitivity of the sign of the longwave heating to the cloud vertical structure is shown in Fig. 16. The calculations employ the refractive indices of ice given in Warren (1984) and the radiative transfer model of Ramaswamy and Kiehl (1985) for a tropical atmospheric profile (McClatchey et al. 1972). The figure shows the heating rate in a layer between 12 and 13 km due to a deep, optically thick, cloud, extending upwards from 3 to 13 km and that due to an anvil type cloud with base at 12 km and top at 13 km. We first note the change in the sign of the longwave effect between the deep and the anvil cloud, irrespective of the ice-water path. This figure demonstrates that the cloud vertical structure governs the sign, while the structure as well as the ice-water path determine the magnitude of the heating. For the particular examples considered here, the magnitude of the longwave effects exceeds the solar effects such that the sign of the net heating is also governed by the cloud vertical structure. The altitude sensitivity is further explored in Table 3 by shifting the cloud tops to 15 and 17 km. The heating rate within the anvil increases substantially as has been pointed out earlier (Ackerman et al. 1988). It is clear that deep clouds cause a cooling while shallow anvil type clouds cause a significant heating of the tropical upper troposphere. Since the areal extent of anvil clouds is significantly greater than the deep clouds in the tropics (Houze and Betts 1981), it is possible that the heating effect may dominate for climatological average conditions, as has been suggested by GCMs (Slingo and Slingo 1988).

In order to gain a perspective of the climatological average conditions, Fig. 17 shows the heating rates in the 12 to 13 km layer for prescribed high, middle and low cloud cover distribution of Manabe and Wetherald (1967, see section 2) with the clouds having a maximum overlap. The longwave effect is still primarily a heating effect but its magnitude is substantially smaller than the values shown in Fig. 16b. This is expected since the intervening low and middle clouds reduce

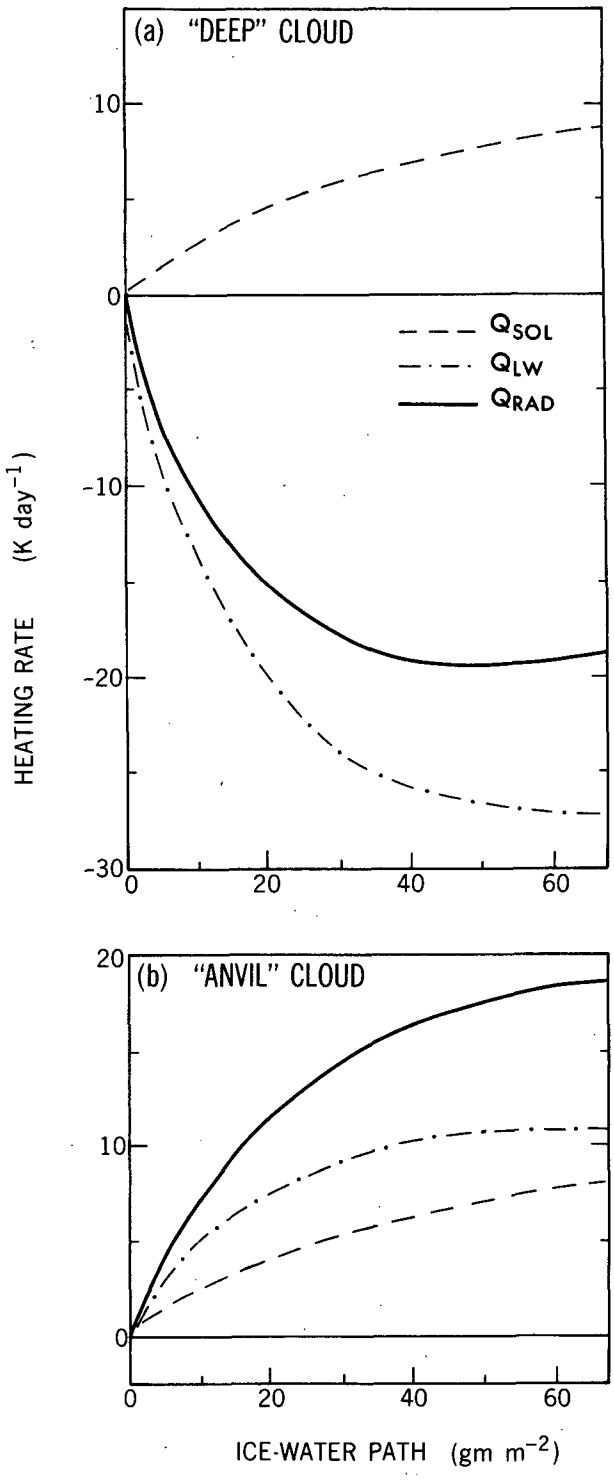

FIG. 16. Heating rates (K d^{-1}) due to solar radiation (Q_{sol}), longwave radiation (Q_{LW}), net radiation (Q_{rad}), as a function of ice-water path (IWP g m^{-2}) in a tropical cirrus cloud located between 12 and 13 km. Case a) corresponds to cirrus as part of an optically thick, vertically extended system ("deep") and case b) corresponds to cirrus cloud located in the upper troposphere with no other clouds below ("anvil").

TABLE 3. Sensitivity of the solar (Q_{sol}), longwave (Q_{LW}) and the net radiative (Q_{rad}) heating rates for a 1-km thick layer to cloud location in the overcast tropical upper troposphere for (a) cirrus cloud as part of an extended cloud system ("deep") and (b) an isolated cirrus cloud over a warm surface ("anvil"). The ice water path is 20 g m^{-2} (see section 7 for details).

	(a) Deep			(b) Anvil-type		
Experiment	Q_{sol} (K d^{-1})	Q_{LW} (K d^{-1})	Q_{rad} (K d^{-1})	Q_{sol} (K d^{-1})	Q_{LW} (K d^{-1})	Q_{rad} (K d^{-1})
Standard (cloud between 12 and 13 km)	4.7	−20.2	−15.5	4.1	7.8	12.9
Same as standard, except:						
(i) cloud between 14 and 15 km	6.1	−20.5	−14.4	5.3	21.6	26.9
(ii) cloud between 16 and 17 km	8.2	−23.4	−15.2	7.0	41.5	48.5

the upwelling radiative flux reaching the cirrus cloud base. Furthermore, excepting for small values of IWP, the solar heating is larger than the longwave heating. The estimates shown in Fig. 17 suggest that both the solar and longwave effect of cirrus can be an important heat source for the tropics. However, the sensitivity calculations here may not include the multitude of possible scenarios which can either make the longwave effect much larger than the value shown in Fig. 17 or alter the sign of the longwave effect. Until a more rigorous database becomes available, it is not possible to be more quantitative on this crucial issue.

8. Summary and conclusions

The principal result of the investigation is the marked significance of cirrus solar absorption to the diabatic heating and the thermal state of the upper troposphere (100–300 mb). The cirrus solar heating is due to the absorption bands of ice in the near-infrared spectrum, and is emphasized by the relatively weak absorption due to the other atmospheric constituents in the upper troposphere. The larger size of the ice crystals (relative to that for water drops) also plays an important role in governing the magnitude of the heating. For example, the solar absorption by a distribution containing large ice crystals exceeds that due to a distribution resembling that of a typical water cloud for condensate paths greater than 20 g m^{-2}. Owing to uncertainties concerning the microphysics, further observational studies of cirrus clouds (in particular, the ice crystal distribution and the IWP) are necessary for future modeling efforts.

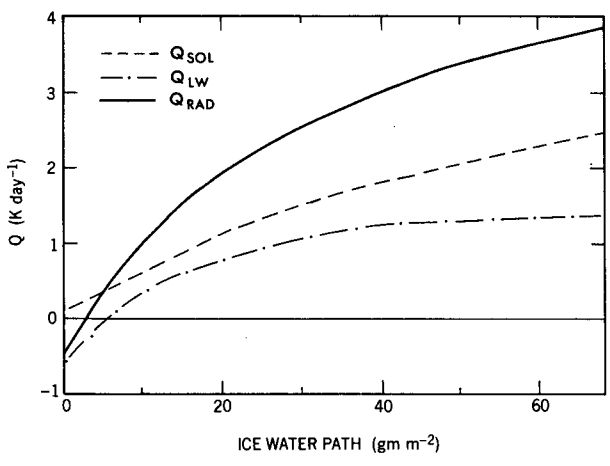

FIG. 17. Heating rates (K day^{-1}) in the 12–13 km layer due to solar radiation (Q_{sol}), longwave radiation (Q_{LW}), net radiation (Q_{rad}) as a function of ice-water path (IWP g m^{-2}), for prescribed cloud cover values of low (0.34), middle (0.08), and high (0.23) clouds.

Observations of ice-water density (IWD) reveal wide variations in the vertical distribution. Solar absorption due to two widely different IWD profiles in the NCAR CCM (January conditions) result in substantial increases in the diabatic heating, particularly in the convective zones. The maximum changes occur in the upper troposphere of the tropics and the high latitudes. At 165 mb, the zonally averaged perturbation is as high as 0.5 K d^{-1} (Fig. 8b). The heating rates are zonally asymmetric, with maxima over the strongly convective regions; for January, the maximum increase in the heating occurs in the Asian monsoonal region (up to 1.5 K d^{-1}). In the tropical belt, the zones of maxima in the computed (by CCM) cirrus solar heating rates match very well the zones of minima in the observed outgoing longwave flux (compare Figs. 3 and 9). Since the minima in the outgoing longwave flux (in the tropics) are caused by upper troposphere cirrus, the above agreement lends some credibility to the regional cirrus cloud fields generated by the CCM.

In the CCM, the cirrus solar absorption enhances the solar heating by more than a factor of two in the tropics (e.g., from 0.28 to 0.70 K d^{-1} at 200 mb, 2.5°S). This increase in the diabatic heating can be one reason for the strong stabilization of the observed lapse rates in the upper troposphere (compare Figs. 2b and 10b).

The magnitude of the computed temperature changes suggests that the lack of cirrus solar absorption could be one reason for the deficiencies in the GCM's

tropical upper tropospheric temperature simulations, particularly above 200 mb (compare Figs. 4, 13 and 15). The strong dependence of the radiative heating on the ice-water path makes it necessary that all aspects of the hydrological processes (moisture transport, cloud formation and dissipation) be simulated correctly in order to rectify the cold bias.

A significant feature of the GCM results is that, although the heating perturbations are over discrete geographical regions, the temperature change is nearly uniform throughout the tropical zone (Fig. 14). The impact of the heating is thus perceived throughout the tropics, contributing to the zonal mean thermal state of the tropical upper troposphere. We recall, at this stage, the results of the Ramanathan et al. (1983) study which, using the same GCM, showed that the cirrus clouds, forming at $P < 200$ mb, have a net heating effect on the tropical upper troposphere. For black cirrus clouds (IWP ≥ 20 g m^{-2}), the computed warming was of the order of 5°K around 200 mb. Thus, the solar heating of cirrus is comparable to its longwave heating, and together their combined heating may indeed be a dominant heat source for the upper troposphere.

It should be cautioned that temperature changes in the upper troposphere due to any change in the diabatic heating depend on the emissivity of the atmosphere and, more particularly, on the cirrus longwave emissivity. Radiation model results illustrate that, for cloud emissivity varying from 0 to 1, the temperature change can vary by as much as 50%. This also points out the need for consistency between short and longwave cloud properties in order to determine the equilibrium thermal state, a point alluded to earlier in a different context by Stephens and Webster (1979).

In contrast to the solar heating in the upper troposphere, the longwave contribution can be one of excessive heating, such as in cirrus decks confined to the upper troposphere and with no clouds below ("anvils") or one of excessive cooling (cirrus cloud as part of a "deep" vertically extended optically thick system), leading to a wide range of possible net radiative contribution. If "anvil" type cirri predominate in the tropical upper troposphere, the magnitude of the longwave warming overwhelms the solar contribution and the effect is accentuated with increasing altitude of cloud location. However, if the actual cloud distribution in the tropics is a mixture of the anvil, deep and lower level cloud systems, resembling the climatological distribution given in Manabe and Wetherald (1967), the magnitude of the longwave heating is reduced and is comparable in magnitude to the cirrus solar heating. These results suggest that, for altitudes above 200 mb, in the tropical zone where observations are sparse and inadequate, the sign of the cirrus radiative heating may be positive on a zonally averaged basis.

The dependence of the radiative processes on ice-water path can hardly be overemphasized. It is because of our poor knowledge of the ice-water path that we are unable to discuss quantitatively the implication of our study to the role of diabatic heating in the upper troposphere general circulation. But, if the climatological ice water path of the upper troposphere clouds is larger than about 10–20 g m^{-2}, our results would imply that the radiative heating due to cirrus clouds is a dominant energy source for the heat budget of the upper troposphere.

Acknowledgments. When this work was begun, both authors were with the National Center for Atmospheric Research. We thank Ms. Gloria Williamson for patiently and laboriously processing the GCM outputs and Dr. J. T. Kiehl for providing us with the tropical temperature profiles of the NCAR CCM. V. Ramanathan's work was funded by the National Science Foundation, Grant ATM8700286. We thank Drs. S. Cox, S. Fels, S. Manabe and one of the reviewers for their detailed comments on the paper.

APPENDIX A

Cirrus Shortwave Absorptivity Parameterization

The expression for absorptivity of a cirrus cloud as a function of cosine of the solar zenith angle (μ) and the optical depth (τ), assuming spherical scatterers and size distribution reported by Heymsfield (1975) is given for $\tau \leq 0.5$, by

$$A(\mu, \tau) = K_1 \tau^a$$

where

$$K_1 = 0.067 + 0.208\mu - 0.983\mu^2 + 1.183\mu^3 - 0.459\mu^4$$

$$a = \min(1, 1.746\mu^{0.463}).$$

For $\tau > 0.5$, the following expression was employed

$$\begin{aligned} A(\mu, \tau) &= 0.5(0.346 + 0.234F_1 - 0.076F_2 + 0.014F_3) \\ &\quad + K_2(0.267 + 0.048F_1 - 0.012F_2 - 0.006F_3) \\ &\quad + K_3(-0.006 - 0.005F_1 + 0.005F_2 - 0.005F_3) \end{aligned}$$

where

$$K_2 = (2\mu - 1.01)/0.99$$

$$K_3 = 2K_2^2 - 1$$

$$F_1 = 0.1\tau - 1$$

$$F_2 = 2F_1^2 - 1$$

$$F_3 = 4F_1^3 - 3F_1.$$

For small optical depth ($\tau < 0.5$), the fits obey a power-law function while for larger values ($\tau > 0.5$), a Chebyshev series, cubic in τ and squared in μ, is employed. The range of the fits is $\tau < 20$ and $\mu > 0.01$.

APPENDIX B

Fixed Dynamical Heating Model

The approach consists of using a one-dimensional, time-marching radiative–convective model (Ramaswamy and Kiehl 1985) with the vertical profiles of temperature, pressure, ozone and water vapor given by the tropical atmosphere profile of McClatchey et al. (1972). Low, middle and high cloud amounts are as given in section 2c. The convective adjustment scheme is turned off; instead, the model is used in the fixed dynamical heating mode (Ramanathan and Dickinson 1979; Fels et al. 1980). Shortwave optical properties of low and middle clouds are as described in section 2c. The shortwave optical property for the high cloud is chosen to yield a heating perturbation similar to that in the GCM (see section 4, Fig. 8b). Clouds are assumed to be either black or grey bodies. Emissivity of low and middle clouds is unity, while that for the high cloud is considered to be a variable.

First, the solar—(Q_{sol}) and the temperature-dependent longwave (Q_{LW}) radiative heating rates are calculated for each layer in the model (see section 2c for details regarding the shortwave transfer and Ramaswamy and Kiehl 1985, for details on the longwave transfer). The dynamical heating rate in each layer (Q_{dyn}) is then assumed to be given by:

$$Q_{dyn}(z) = -[Q_{sol}(z) + Q_{LW}(z)].$$

With Q_{dyn} defined thus, the model is in radiative-dynamical equilibrium, i.e.,

$$Q(z) = Q_{sol}(z) + Q_{LW}(z) + Q_{dyn}(z) = 0.$$

Next, a shortwave perturbation due to the presence of a cirrus cloud (located at a layer denoted by z_c) is considered, i.e.,

$$Q'_{sol}(z_c) = Q_{sol}(z_c) + \delta Q_{sol}(z_c).$$

This is the forcing applied to the model atmosphere in radiative–dynamical equilibrium. Note that this heating perturbation could equally well represent any other component of the diabatic heating (e.g., latent heat release). We choose a magnitude of perturbation based on the maximum value appearing in Fig. 8b (FC case; ~ 0.5 K day^{-1}). Two different high-cloud altitudes are considered (i) cloudtop at 13.6 km (165 mb) and cloudbase at 12 km (217 mb) and (ii) cloudtop at 12 km (217 mb) and cloudbase at 10.4 km (267 mb). The application of a thermal forcing in any model layer perturbs the basic radiative–dynamical equilibrium ($Q \neq 0$). This alters the temperatures which, in turn, alters the longwave cooling rates.

The model atmosphere is then time marched, using a time step (Δt) of three hours (keeping ground temperature, water vapor, solar and dynamical heating rates fixed). At each time step, new temperatures (T) are computed for all layers according to

$$T(z) = T(z) + Q(z)\Delta t$$

where

$$Q(z) = Q'_{sol}(z) + Q'_{LW}(z) + Q_{dyn}(z)$$

with the primes denoting the quantities in the perturbed state. After the determination of the temperatures at each time step, the new longwave cooling rates are calculated.

The time marching procedure is continued until a new equilibrium thermal profile is established such that $Q(z)$ is again 0 for all z, i.e.,

$$Q'_{LW}(z) = -Q'_{sol}(z) - Q_{dyn}(z)$$
$$= Q_{LW}(z) - \delta Q_{sol}(z).$$

In the numerical calculation, the criterion for equilibrium is that the sum of the radiative and dynamical heating (Q) be less than or equal to 10^{-4} K d^{-1} in all layers.

The change in temperature at z_c between the old and the new radiative–dynamical states is the radiative response at the location of the cloud to the imposed perturbation.

REFERENCES

Ackerman, T. P., K. N. Liou, F. P. J. Valero and L. Pfister, 1988: Heating rates in tropical anvils. *J. Atmos. Sci.*, **45**, 1606–1623.

Albrecht, B. A., V. Ramanathan and B. A. Boville, 1986: The effects of cumulus moisture transports on the simulations of climate with a general circulation model. *J. Atmos. Sci.*, **43**, 2443–2462.

Boville, B. A., 1987: The validity of the geostrophic approximation in the winter stratosphere and troposphere. *J. Atmos. Sci.*, **44**, 443–457.

Charlock, T. P., and V. Ramanathan, 1985: The albedo field and cloud radiative forcing produced by a general circulation model with internally generated cloud optics. *J. Atmos. Sci.*, **42**, 1408–1429.

Chylek, P., V. Ramaswamy and R. Cheng, 1984: Effect of graphitic carbon on the albedo of clouds. *J. Atmos. Sci.*, **41**, 3076–3084.

Cox, S. K., and K. T. Griffith, 1979: Estimates of radiative divergence during Phase III of the GARP Atlantic Tropical Experiments. Part II: Analysis of Phase III results. *J. Atmos. Sci.*, **36**, 586–601.

Donner, L. J., 1986: Sensitivity of the thermal balance in a general circulation model to a parameterization for cumulus convection with radiatively interactive clouds. *J. Atmos. Sci.*, **43**, 2277–2288.

Fels, S. B., 1985: Radiative-dynamical interactions in the middle atmosphere. *Advances in Geophysics*, Vol. 28A, Academic Press, 277–300.

——, and L. D. Kaplan, 1975: A test of the role of longwave radiative transfer in a general circulation model. *J. Atmos. Sci.*, **33**, 779–789.

——, J. D. Mahlman, M. D. Schwarzkopf and R. W. Sinclair, 1980: Stratospheric sensitivity to perturbation in ozone and carbon

dioxide: Radiative and dynamical response. *J. Atmos. Sci.*, **37**, 2265–2297.

Fleming, J. R., and S. K. Cox, 1974: Radiative effects of cirrus clouds. *J. Atmos. Sci.*, **31**, 2182–2188.

Griffith, K. T., S. K. Cox and R. G. Knollenberg, 1980: Infrared radiative properties of tropical cirrus clouds inferred from aircraft measurements. *J. Atmos. Sci.*, **37**, 1077–1087.

Heymsfield, A., 1975: Cirrus uncinus generating cells and the evolution of cirriform clouds. Part I: Aircraft observations of the growth of the ice phase. *J. Atmos. Sci.*, **32**, 799–808.

——, 1977: Precipitation development in stratiform ice clouds: A microphysical and dynamical study. *J. Atmos. Sci.*, **34**, 367–381.

Holton, J. R., 1979: *An Introduction to Dynamic Meteorology*, 2nd ed., Academic Press, 333–335.

Houze, R. A., 1982: Cloud clusters and large-scale vertical motions in the tropics. *J. Meteor. Soc. Japan*, **60**, 396–410.

——, and A. K. Betts, 1981: Convection in GATE. *Rev. Geophys. Space Phys.*, **19**, 541–576.

Kley, D., A. L. Schmeltekopf, K. Kelly, R. H. Winkler, T. L. Thompson and M. McFarland, 1982: Transport of water through a tropical tropopause. *Geophys. Res. Lett.*, **9**, 617–620.

Kratz, D. P., and R. D. Cess, 1985: Solar absorption by atmospheric water vapor: a comparison of radiation models. *Tellus*, **37B**, 53–63.

Liou, K., 1973: Transfer of solar irradiance through cirrus cloud layers. *J. Geophys. Res.*, **78**, 1409–1418.

——, 1986: Influence of cirrus clouds on weather and climate processes: a global perspective. *Mon. Wea. Rev.*, **114**, 1167–1199.

——, and T. Sasamori, 1975: On the transfer of solar radiation in aerosol atmospheres. *J. Atmos. Sci.*, **32**, 2166–2177.

——, and C. D. Wittman, 1979: Parameterization of the radiative properties of clouds. *J. Atmos. Sci.*, **36**, 1261–1273.

Mahlman, J. D., and L. Umscheid, 1984: Dynamics of the middle atmosphere: Successes and problems of the GFDL "SKYHI" general circulation model. *Dynamics of the Middle Atmosphere*, J. R. Holton and T. Matsuno, Eds., Terra Scientific, 501–525.

Manabe, S., and R. Wetherald, 1967: Thermal equilibrium of the atmosphere with a given distribution of relative humidity. *J. Atmos. Sci.*, **24**, 241–259.

——, and ——, 1980: On the distribution of climate change resulting from an increase in CO_2 content of the atmosphere. *J. Atmos. Sci.*, **37**, 99–118.

McClatchey, R. A., R. W. Fenn, J. E.A. Selby, F. E. Volz and J. S. Garing, 1972: *Optical Properties of the Atmosphere*, third ed., AFCRL-72-0497, Air Force Cambridge Research Laboratories, Hanscom AFB, MA, 110 pp.

Newell, R. E., J. W. Kidson, D. G. Vincent and G. J. Boer, 1974: *The General Circulation of the Tropical Atmosphere*, Vol. 2. The MIT Press, Chapters 6 and 7, p. 1–54.

Oort, A. H., and E. M. Rasmusson, 1971: Atmospheric circulation statistics. NOAA Prof. Paper 5, U.S. Department of Commerce, U.S. Govt. Printing Office, Washington DC, 323 pp.

Paltridge, G. W., and C. M. R. Platt, 1981: Aircraft measurements of solar and infrared radiation and the microphysics of cirrus clouds. *Quart. J. Roy. Meteor. Soc.*, **107**, 367–380.

Pitcher, E. J., R. C. Malone, V. Ramanathan, M. L. Blackmon, K. Puri and W. Bourke, 1983: January and July simulations with a spectral general circulation model. *J. Atmos. Sci.*, **40**, 580–604.

Plumb, R. A., D. G. Andrews, M. A. Geller, W. L. Grose, A. O'Neill, M. Salby and R. A. Vincent, 1986: Dynamical Processes. *Atmospheric Ozone 1985*, Vol I, Global Ozone Research and Monitoring Project, Rep. No. 16, World Meteorological Organization, Geneva, Switzerland, 241–347.

Ramanathan, V., 1987: Atmospheric general circulation and its low frequency variance: Radiative influences. *J. Meteor. Soc. Japan*, **65**, 151–175.

——, and R. E. Dickinson, 1979: The role of stratospheric ozone in the zonal and seasonal radiative energy balance of the earth-troposphere system. *J. Atmos. Sci.*, **36**, 1084–1104.

——, and P. Downey, 1986: A nonisothermal emissivity and absorptivity formulation for water vapor. *J. Geophys. Res.*, **91**, 8649–8666.

——, E. J. Pitcher, R. C. Malone and M. L. Blackmon, 1983: The response of a general circulation model to refinements in radiative processes. *J. Atmos. Sci.*, **40**, 605–630.

Ramaswamy, V., and J. T. Kiehl, 1985: Sensitivities of the radiative forcing due to large loadings of smoke and dust aerosols. *J. Geophys. Res.*, **90**, 5597–5613.

——, and A. Detwiler, 1986: Interdependence of radiation and microphysics in cirrus clouds. *J. Atmos. Sci.*, **43**, 2289–2301.

Riehl, H., 1950: On the role of the tropics in the general circulation of the atmosphere. *Tellus*, **20**, 1–17.

Slingo, A., and J. M. Slingo, 1988: The response of a general circulation model to cloud longwave radiative forcing. Part I: Introduction and initial experiment. *Quart. J. Roy. Meteor. Soc.*, **114**, 1027–1062.

Stephens, G. L., 1980: Radiative properties of cirrus clouds in the infrared region. *J. Atmos. Sci.*, **37**, 435–446.

——, and P. J. Webster, 1979: Sensitivity of radiative forcing to variable cloud and moisture. *J. Atmos. Sci.*, **36**, 1542–1556.

Warren, S. G., 1984: Optical constants of ice from the ultraviolet to the microwave. *Appl. Opt.*, **23**, 1206–1225.

Washington, W. M., and G. A. Meehl, 1984: Seasonal cycle experiments on the climate sensitivity due to a doubling of CO_2 with an atmospheric general circulation model coupled to a simple mixed layer ocean model. *J. Geophys. Res.*, **89**, 9475–9503.

Webster, P. J., and G. L. Stephens, 1980: Tropical upper troposphere extended clouds: Inferences from winter MONEX period. *J. Atmos. Sci.*, **37**, 1521–1541.

Williamson, D. L., J. T. Kiehl, V. Ramanathan, R. E. Dickinson and J. J. Hack, 1987: Description of NCAR commuity climate model (CCM1). NCAR Tecnical Note NCAR/TN-285+STR, National Center for Atmospheric Research, Boulder, CO.

Wiscombe, W. J., 1977: The Delta-Eddington approximation for a vertical inhomogeneous atmosphere. NCAR technical note NCAR/TN-121+FTR, NCAR, Boulder, CO, 66 pp.